Amoxicillin encapsulation on alginate/magnetite composite and its antimicrobial properties against gram-negative and positive microbes

Owolabi M. Bankole[1*], Kehinde I. Ojubola[2], Olayinka S. Adanlawo[2], Abiola O. Adesina[3], Idris O. Lawal[2], Adeniyi S. Ogunlaja[1], Ojodomo J. Achadu[4]

[1]Department of Chemistry, Nelson Mandela University, Port Elizabeth, South Africa.

[2]Hydrochemistry Research Laboratory, Adekunle Ajasin University, Akungba, Nigeria.

[3]Department of Chemical Sciences, Adekunle Ajasin University, Akungba, Nigeria.

[4] School of Health and Life Sciences, and National Horizon Centre, Teesside University, TS1 3BA, Middlesbrough, United Kingdom.

Abstract

The current paper describes the use of a sodium alginate stabilized magnetite (AFe) nanocomposite to encapsulate amoxicillin (AMX) as an antibacterial therapy against gram-positive and gram-negative bacteria, *Listeria monocytogenes* and *Salmonella typhi*, respectively. The use of alginate provides various functional groups and expanded active sites for the composite to adsorb amoxicillin via stable electrostatic interactions. A variety of imaging and spectroscopic techniques were used to analyze the as-synthesized alginate-capped magnetite (AFe) before and after composition with amoxicillin (AMX). The results of percentage loading capacity and encapsulation efficiency suggest that significant active contents of AMX were adsorbed onto AFe to afford alginate stabilized magnetite-loaded amoxicillin (AFeAMX) during loading experiments, and that these active components were released in two stages: first, via an initial burst lasting for 2 h, followed by a continuous and sustained release of AMX lasting over 48 h. The in vitro release profiles show that 86.4 % and 74.6% of AMX are respectively released from the formulation at pH 6.2 and 7.4 after 96 h. Antimicrobial efficacy of AFe composited with AMX is more pronounced against *L. monocytogenes,* with higher inhibitory growth effect at lower AFeAMX dosages than against gram-negative bacterium of *S. typhi.* The results suggest that gram-negative bacteria had higher antimicrobial resistance to the amoxicillin-loaded alginate-magnetite composite than gram-positive bacteria.

Keywords: magnetite-alginate; amoxicillin; antimicrobial; *Listeria monocytogenes*; *Salmonella typhi*; bacteria.

*Corresponding author. Tel: + 2348034018955; E-mail: bankolemutolib@yahoo.com.

Introduction

Nanotechnology or nanoscience has gained a lot of appeal among researchers due to the possibility of fabricating nano-sized materials with large surface areas and improved physico-chemical properties compared to the same materials in bulk [1]. The increased surface area of nanomaterials provides more active sites for therapeutic medications such as anticancer, antiviral, antifungal, and antibacterial to be encapsulated and shielded from harsh environmental conditions [2, 3]. The stealthy properties of these formulations enable for a sustained and regulated delivery of the medications to the targeted organs or tissues in the body [2, 4, 5].

Antiviral, antifungal, and antibacterial nano delivery systems based on tailor-made nanomaterials are the most researched and reported in the literature, with the latter being more common due to the ease and cost-effectiveness of the microbiological testing methods for bacteria [6, 7]. Furthermore, because bacteria are single-celled organism, their infections are easily treated with antibiotics, in contrast to viral and fungal infections, which have shown to be more difficult and complicated to treat due to the diversity of their structures and properties [6, 7]. Due to its simple technique of synthesis, low toxicity, and simplicity of recovery of the materials after reaction using an external magnetic field, magnetite and its composites are the most notable nanomaterials that have been described for loading antibiotic medicines for antimicrobial research [8, 9]. The most notable modes of antimicrobial activity of iron based nanoparticles are adhesion of nanoparticles to microbial cell walls, release and bioaccumulation of toxic metal ions in bacteria cells, and stimulation of pathogen destruction through formation of reactive oxygen species such as superoxide, hydrogen peroxide, and hydroxyl radical [8–12].

Grumezescu *et al* [12] reported the synthesis of amoxicillin stabilized magnetite nanostructures (Fe_3O_4@AMO) and demonstrated that the fabricated drug delivery system has a lower minimum inhibitory concentration (MIC) against the tested isolates than the standard amoxicillin. It's worth noting that bare magnetite nanoparticles have poor surface textural properties, and a significant inclination to agglomerate when exposed to air [13, 14]. As a result, its application in adsorption studies without stabilizers is highly restricted. According to literature reports, stabilizing the surface of magnetite NPs with biopolymers like sodium alginate is advantageous because it has a

high binding capacity with Fe_3O_4, can expands the surface catalytic active sites of Fe_3O_4 and endows the surface of the new composite with a large number of functional groups for rapid adsorption of adsorbate in aqueous solution [14].

In the literature, stable interactions between amoxicillin and sodium alginate have been documented, with strong electrostatic contacts being attributed to the mode of interactions [15, 16]. Thus, for the first time, the use of sodium alginate-capped magnetite (AFe) for amoxicillin (AMX) loading and its antimicrobial efficacy against *Listeria monocytogenes* (gram-positive bacteria) and *Salmonella typhi* (gram-negative bacteria) is reported in the current study. Using the standard co-precipitation approach, the current study reports a one-pot method for synthesizing sodium alginate stabilized magnetite nanoparticles in natural air. The resulting nanocomposite was utilized as an adsorbent to load amoxicillin in aqueous solution. Amoxicillin is a semi-synthetic amino-penicillin antibiotic that belongs to the family of penicillins and differs from the parent antibiotic only in the hydroxylation of acylamino side chain, Figure 1 [17]. In comparison to penicillin, amoxicillin is a broad-spectrum antibiotic that is effective against both gram-positive and gram-negative bacteria. Amoxicillin kills bacteria by inhibiting the formation of cell walls in microorganisms [17]. Antimicrobial therapy using a combination of amoxicillin and an alginate-magnetite composite is proposed here against gram-positive (*L. monocytogenes*) and gram-negative (*S. typhi*) bacteria.

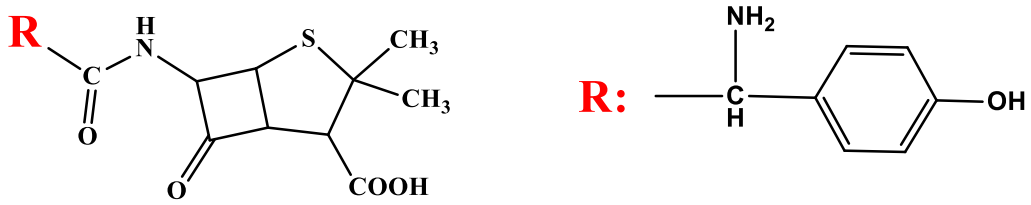

Figure 1: The structural formula of Penicillin and R group depicting the hydroxylation of acyl side chain.

2.0 Materials and methods

2.1 Materials

Iron (II) chloride tetrahydrate (ReagentPlus®, 98%), Iron (III) chloride hexahydrate (ACS reagent, 97%), potassium nitrate (KNO_3, analytical reagent), sodium hydroxide (ACS reagent, ≥ 97.0%,

pellets) and sodium alginate were purchased from Loba Chemie PVT LTD. Ammonium hydroxide ($NH_4OH; 28\%\ w/w$), sulfuric acid solution (98%), amoxicillin (potency: ≥900 μg/mg) were purchased from Pascal Scientific Limited. All the reagents were used as received. High purity deionized water was used throughout the experiments.

2.2 Methods

2.2.1 Preparation of sodium alginate-capped magnetite nanoparticles (AFe).

Sodium alginate-capped magnetite nanoparticles **(**denoted as AFe) was prepared through one-pot co-precipitation method [18, 19], but with minor modification. Ferric and ferrous chlorides were used as the sources of $Fe^{3+}$and Fe^{2+} ions at 2: 1 mole ratio, respectively.Briefly,$FeCl_2.4H_2O$ (10.8 mmol, 2.15 g) and$FeCl_3.6H_2O$ (21.6 mmol, 5.83 g) were measured and added into180 mL of ethanol and water ($v: v;\ 1: 2$) mixture, then 0.3 g of sodium alginate was added and the mixture was sonicated for 1 h to ensure complete dissolution of the iron salts and sodium alginate. Thereafter, the mixture was transferred to magnetic hotplate and heated to 80 ℃ for 30 min under vigorous stirring. Then 15 mL of ammonia solution was added to the mixture drop wise to adjust the pH to 13. The crude solution was stirred further for another 1 h and the brown-black color precipitate which indicates formation of sodium alginate-capped magnetite composite was recovered from the solution through external magnet and washed repeatedly with deionized water and ethanol by centrifuge, and then dried in the oven at 60 ℃ overnight. TGA curves were used to determine the alginate content of bare magnetite, which was prepared under similar conditions as AFe NPs but without sodium alginate.

2.2.2 Amoxicillin loading on alginate-magnetite composite.

Sodium alginate (1g) was ground into powder and dispersed in 100 mL of water in 250 mL beaker and sonicated for 2h. Then, 0.3 g of amoxicillin (AMX) was added to the aqueous solution of AFe solution and stirred for 30 min to facilitate AMX uptake onto AFe. The pH of the solution was adjusted to 10 by 0.1 M NaOH and the mixture was magnetically stirred for 48 h. The AFe loaded with AMX (AFeAMX) were separated by an external magnet, and the non-encapsulated AMX in the filtrate solution was filtered using 0.2 micron filter paper. The recovered AFeAMX was washed with water and dried at 50 ^oC for 12 h for further studies.

2.2.2.1 Percentage encapsulation efficiency (%EE)

Encapsulation efficiency (EE) is a term used to measure the exact amount of antibiotic encapsulated by nanoparticles or adsorbents after loading [20, 21]. It is determined by subtracting the non-encapsulated AMX (in the filtrate) from the total weight of AMX fed before the adsorption studies per total weight of AMX used for adsorption. To determine the EE of AMX on AFe after loading, the unbounded AMX in the filtrate was extrapolated from the standard calibration curve [$y = 0.0213x + 0.004$; $r^2 = 0.999$] of known concentrations of amoxicillin solutions ranging from $5 - 30$ mg/L at a wavelength of 275 nm, Figure 2, corresponding to maximum absorbance peak of amoxicillin ($\lambda_{max}$of AMX) [22, 23] on UV-Vis spectrophotometer. The encapsulation efficiency (%EE) of AMX on AFe was determined using **Eqn. 1** [21].

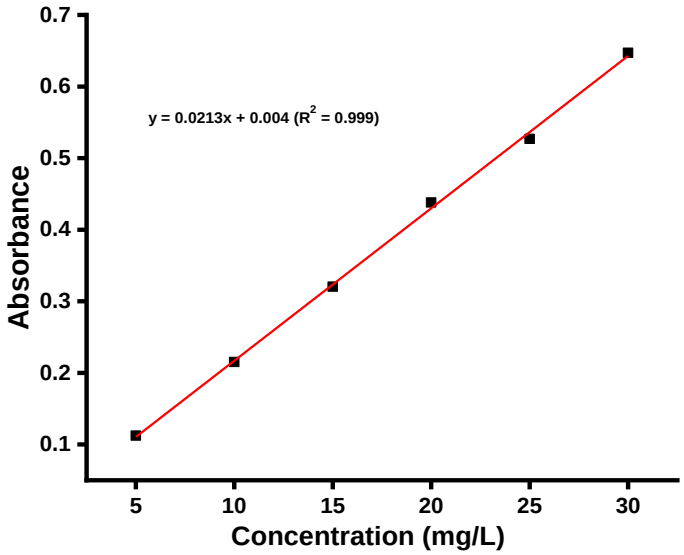

Figure 2: Standard calibration curve for amoxicillin (AMX) at concentrations ranging from $5 - 30$ mg/L in deionized water.

$$\% \text{ Encapsulation efficiency} = \frac{W_{total} - W_{left}}{W_{total}} \times 100 \qquad \textbf{1}$$

where $W_{total}$is the total mass of AMX for adsorption studies and $W_{left}$is the mass of AMX in the filtrate after loading.

2.2.2.2 Percentage loading capacity (%LC)

The loading capacity measures the amount of encapsulated AMX per unit weight of the adsorbent (AFe). The loading capacity is also expressed as percentage and thus, the loading content of AMX on AFe is calculated using **Eqn. 2** [23, 24], and refers to the amount of AMX entrapped by the total weight (1 g) of AFe after loading.

$$\%\ \text{AMX loading capacity} = \frac{W_{total} - W_{left}}{W_{\text{AFe}}} \times 100 \qquad \mathbf{2}$$

where $W_{\text{AFe}}$is the total mass of AFe used as adsorbent for AMX, $W_{total}$and W_{left}as explained above.

2.2.3 In vitro release study of AMX from alginate-magnetite composite.

Phosphate buffer solutions (PBS) at pH 6.2 and 7.4 were used as dissolution media for in vitro release of amoxicillin from amoxicillin-loaded AFe nanoparticles in a 100 mL conical flask. Typically, 20 mg of AFeAMX was dispersed separately in 50 ml of PBS with pH 6.2 and 7.4, and the mixtures were stirred at 80 rpm for 96 h at $37 \pm 0.6℃$ on a magnetic hotplate stirrer. 3 mL of the samples were withdrawn periodically from the AMX-NPs-mixture at time (t) = 0, 1, 2, 4, 6, 8, 10, 12, 14, 16, 18, 20, 24, 30, 34, 40, 44, 48, 54, 60, 65, 72, 80, 96 h, and replaced with the same volume (3 mL) of fresh PBS (pH 6.2 or 7.4) to keep the volume of the solution constant. The quantity of AMX released by the AFeAMX composite was analyzed on UV-visible spectrophotometer at 275 nm, and the cumulative release profile was plotted against time (t). The percent release of AMX was also measured using **Eqn. 3**:

$$\text{AMX release (\%)} = \frac{W_{AMX}}{W_{AFeAMX}} \times 100 \qquad \mathbf{3}$$

where W_{AMX} and $W_{AFeAMX}$are respectively the amounts of AMX released and the amount of AMX loaded used for the release study.

2.2.4 Determination of pH of point zero charge (pH PZC)

The pH of point zero charge (PZC) was determined using the solid addition method viz: to a series of 100 mL conical flasks, 40 mL of 0.1M KNO_3 solution was transferred. The initial pH (pH_o) values of the solution were adjusted from 2 to 10 by adding either 0.1N H_2SO_4 or NaOH. The total

volume of the solution in each flask was made exactly to 50 mL by adding the KNO_3 solution. Then 0.05 g of nanoparticles was added to each flask and securely capped immediately. The suspension was then manually agitated for 24h. The pH values of the supernatant liquid were noted after 24 h and denoted as pH_f. The difference between the initial (pH_o) and final pH (pH_f) values ($\Delta pH = pH_o - pH_f$) was plotted against the pH_o, and the point of intersection of the resulting curve at zero gave the PZC.

2.2.5 Bacterial culture and test isolates

The nutrient agar medium for the bacterial culture was first homogenized by boiling to dissolve all the components; and then autoclaved for 15 min at ~121^{o}C. The medium was allowed to cool to temperature of about 45^{o}C and the content was poured into petri-dish. The petri-dish plates were allowed to solidify before inoculation. Two clinical organisms which includes and *Listeria monocytogenes* (gram-positive bacteria) and *Salmonella typhi* (gram-negative) were received from Department of Microbiology, Adekunle Ajasin University, Akungba, Nigeria. The biochemical and morphological characteristics of the clinical isolates were elucidated using the conventional morphological, cultural and biochemical characterization according to Bergey's manual of determinative bacteriology 9th edition. The bacterial cultures were maintained on nutrient broth. Inoculum size containing 1.5x10^8 CFU/ml (0.5 McFarland standard) of each bacterium was used to seed already solidified petri-dish plates. The bacterial plates were incubated at 37^{o}C overnight.

2.2.6 Antimicrobial susceptibility test

The antimicrobial activities of sodium alginate, bare magnetite nanoparticles, as-prepared AFe nanoparticles before and after loading of AMX were elucidated using agar well diffusion method. A sterile 6mm cork borer was used to make five (5) wells on the solidified agar for deionized water as negative control and known concentrations of sodium alginate, AFe composite, amoxicillin and AFeAMX composite. The minimum inhibitory concentrations (MICs) and minimum bactericidal concentrations (MBCs) which refer to the lowest concentrations of the antimicrobial samples that will inhibit the visible growth or kill the bacterium cells of the tested isolates, respectively, are determined using a method described by Akinpelu *et al* [25]. Serial dilutions of the prepared samples were carried out to give concentrations ranging from1 μg/mL to 200μg/mL. From each diluted concentration, 2 mL was measured and added to 18mL of pre-sterilized molten Mueller-

hinton, properly mixed and allowed to set. The standardized inoculums were seeded on the plates and the bacterial plates were incubated at 37^{o}C for 24 h. After incubation period of 24 h, the MIC and MBC results, which indicate no formation of turbidity or apparent growth of the tested isolates were observed and compared to the control tubes (deionized water).

2.3. Material characterizations

The solid reflectance spectra of amoxicillin, alginate-capped magnetite (AFe) nanoparticles and amoxicillin-loaded AFe (AFeAMX) were recorded on a Shimadzu UV-VIS-NIR Spectrophotometer UV-3100 with a MPCF-3100 sample compartment with samples mounted between two quartz discs which fit into a sample holder coated with barium sulfate. The spectra were recorded over the wavelength range of 250-800 nm, and the scans were conducted at a medium speed using a 20 nm slit width. Infra-red spectra of prepared samples were recorded on a Thermo Fisher Scientific FTIR spectrophotometer, using pressed KBr pellets. Transmission electron microscope (TEM) images of the samples (AFe and AFeAMX) were recorded using a JEOL JEM-2010 electron microscope operating at 200 KV. Scanning electron microscope (SEM) XL 30 FEG ESEM was used to elucidate the surface morphologies of AFe and AFeAMX. X-ray photoelectron spectroscopy (XPS) analysis of the AFe was performed on a Kratos Axis Ultra X-ray Photoelectron Spectrometer equipped with a monochromatic Al K_{α} source (1486.6 eV). The BET Surface area was measured using Micrometrics TriStar II 3020 Surface Area Analyzer. Thermal stabilities of the samples were performed using a Perkin Elmer STA 6000 with a thermocouple sensor Pt-Pt/Rh. Samples were loaded onto a crucible pan and heated under N_2 atm from 30-800°C at a flow rate of 25.00°C/min. The hydrodynamic size distributions of AFe NPs, AFeAMX composite and AMX were measured using Malven Dynamic Light Scattering (DLS), Malven, UK.

3.0 Results and Discussions

3.1.1 Scanning and transmission electron microscope

The sodium alginate capped magnetite nanoparticles and AMX-loaded magnetite composite visualized under scanning electron microscope are shown Figure 3 (a&b). Figure 3a shows that the surface of alginate capped magnetite nanoparticles has rough surfaces with different contours. The particles are overlaid due to aggregation and revealed irregular shapes and sizes. The SEM

image of magnetite loaded with AMX in Figure 3b showed smooth surface which is in contrast to the surface of SEM image of unloaded magnetite nanoparticles in Figures 3a. The smoother surface of AFeAMX could be attributed to the effect of prolonged sonication and dispersion of the amoxicillin on magnetite nanoparticles. The transmission electron microscope revealed that AFe is pseudo-spherical in shape and slightly agglomerated as shown in Figures 3c. The TEM image observed for AFeAMX showed agglomerated particles due to the presence of amoxicillin on magnetite nanoparticles. The transmission electron microscope revealed that AFe is pseudo-spherical in shape and slightly agglomerated as shown in Figures 3c. The TEM image observed for AFeAMX showed agglomerated particles due to the presence of amoxicillin on magnetite nanoparticles.

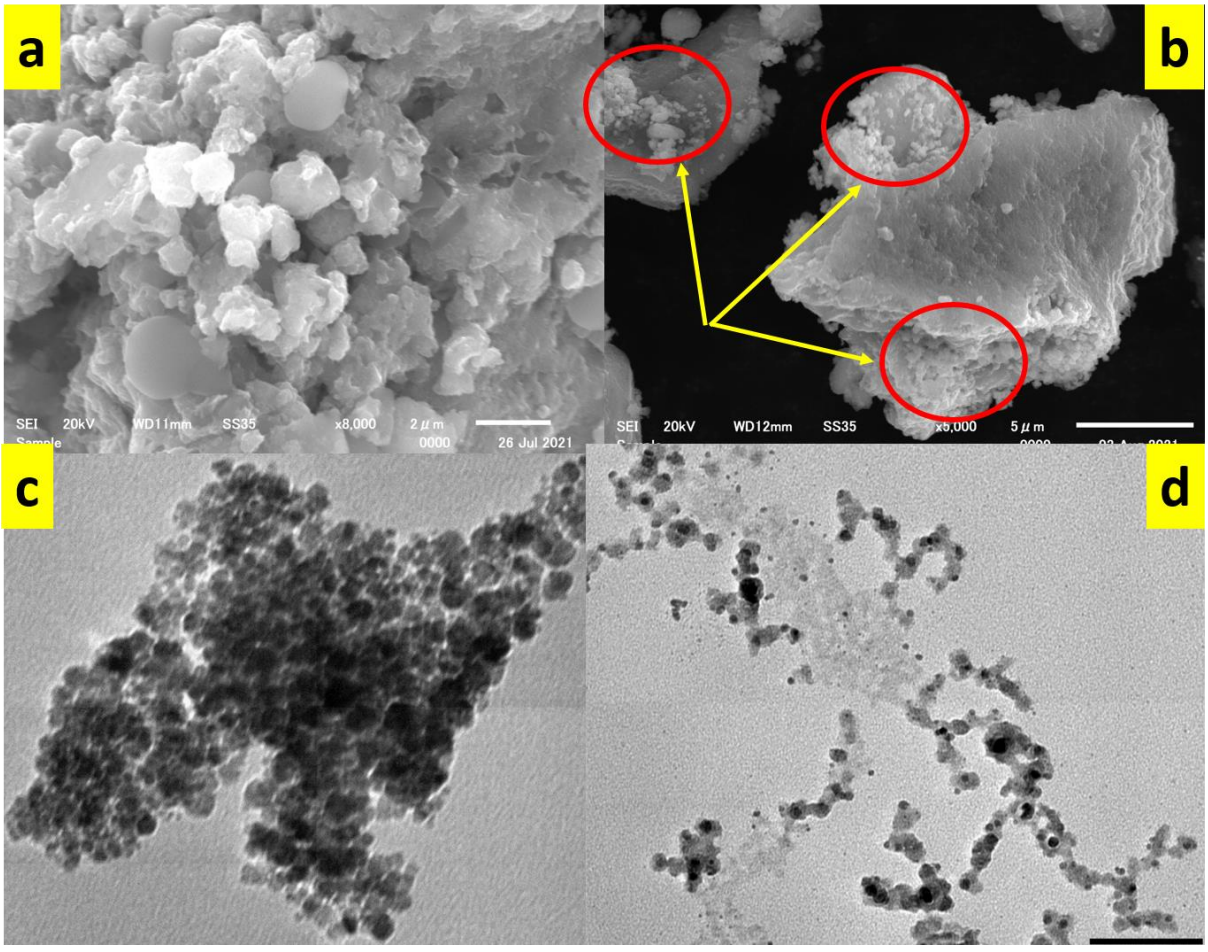

Figure 3: (a) SEM image of AFe (b) SEM image of AFeAMX (c) TEM image of AFe (d) TEM image of AFeAMX.

3.1.2 Dynamic light scattering.

The hydrodynamic size distribution of AMX,AFe nanoparticles and AMX loaded magnetite composite was elucidated using dynamic light scattering (DLS), Figure 4. The result revealed that the hydrodynamic peak diameter of bare AFe ranges from 210 to 240 nm with an intense average hydrodynamic peaked at ~229 nm, while hydrodynamic peak diameter of AMX was observed between 500 and 2000 nm with an average diameter peaking at 1000 nm. Interestingly, upon adsorption of AMX onto AFe nanoparticles forming AFeAMX, the hydrodynamic peak was observed between 230 to 700 nm with an average particle size of 330 nm. The significant shift in the hydrodynamic peak from 229 to 330 nm and the corresponding reduction in the intensity peak after AMX loading on AFeAMX is an indication that the amoxicillin has been successfully loaded on the AFe nanoparticles.

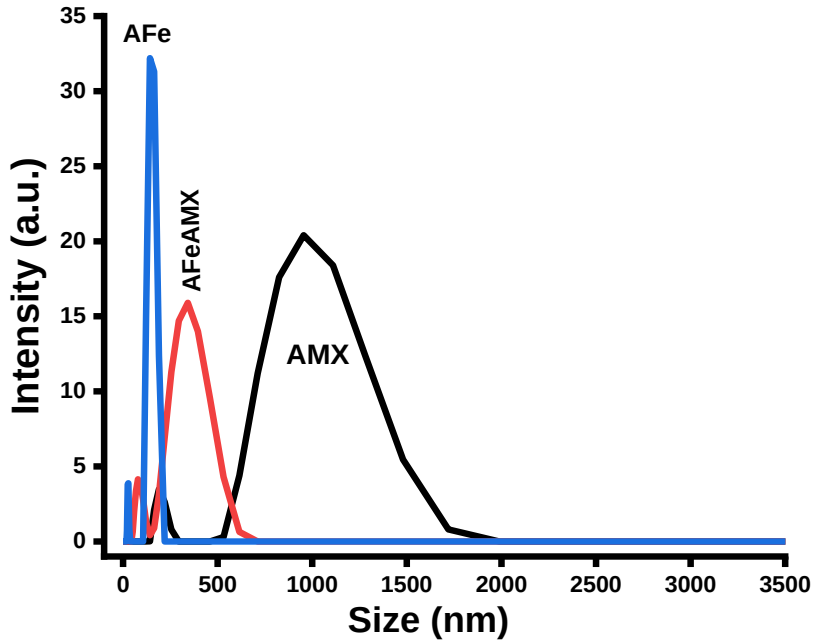

Figure 4: Dynamic light scattering (DLS) measurements of AFe nanoparticles, AFeAMX composite and AMX.

3.1.3 Optical absorption characterizations

Normalized UV-Vis diffuse reflectance spectra of AFe nanoparticles, AFeAMX composite and AMX are shown in Figure 5. The optical absorption of AFe covers the entire ultra violet and visible regions without clear absorption band. Similar results have been reported in the literature.

Absorption spectrum of AMX shows a strong and wide optical absorption intensity spreads around 300 to 400 nm and peaked at 345 nm in the UV due to the $\pi \rightarrow \pi^*$ electronic transitions [26]. After the loading of the AMX on AFe, a maximum absorption intensity and a threshold absorption band around 350-420 nm due to the presence of AMX was observed in the UV spectrum of AFeAMX. The absorption peak of AMX in the AFeAMX red shifted to 373 nm, suggesting that the AMX was successfully loaded on AFe.

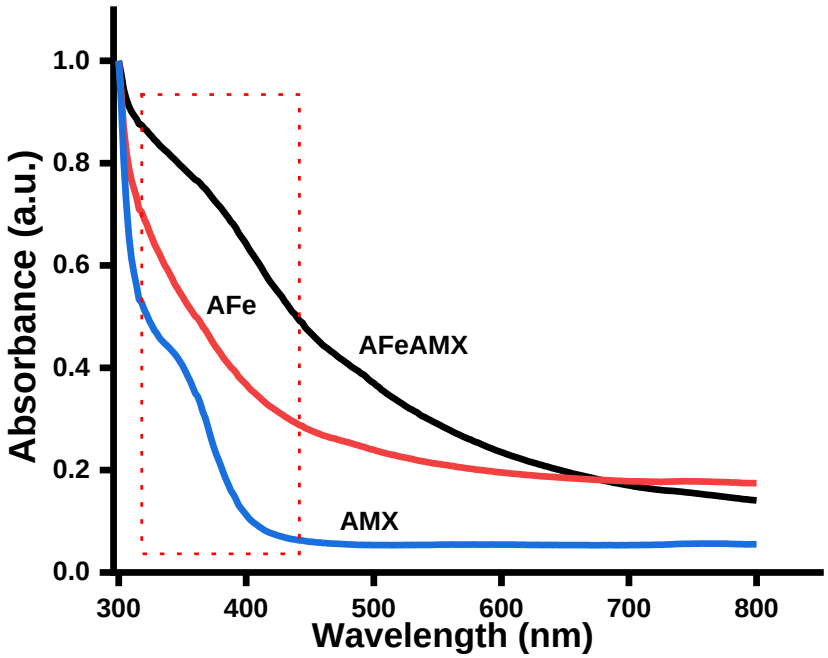

Figure 5: UV spectra of AFe nanoparticles, AFeAMX composite and AMX

3.1.4 Phase pattern and structure analysis

The phase structural patterns of AMX, AFe nanoparticles and AFe composited with AMX were determined using Powdered X-ray diffraction analysis and the results are shown in Figure 6. The X-ray patterns of AMX revealed high crystalline patterns with reflections at $2\theta = 15.3°, 16.9°, 18.8°, 22.1°, 26.1°$ and $28.1°$. The result is consistent and in good agreements with previous reports on PXRD analysis of pure amoxicillin [27–29]. The diffractogram of AFe shows crystalline Bragg's diffraction peaks at $2\theta = 30.50°\ 35.45°, 43.34°, 53.50°$, and $58.10°$, corresponding to the 220, 311, 400, 422, 511 reflection planes which are indexed to the inverse spinel planes of Fe_3O_4(JCPDS Card No. 79-0417) [30]. The diffraction patterns of AFeAMX are similar to that of AFe, except for the broadness and slight reduction in the diffraction patterns of

AFeAMX compared to AFe, which is attributed to the presence of AMX in the former. This confirm that there was no destruction to the crystallinity of the magnetite nanoparticles after AMX loading. It is noteworthy to mention that the diffraction peaks of AMX are conspicuously absent in the PXRD patterns of AFeAMX. Similar observation has been reported in the literature [27].

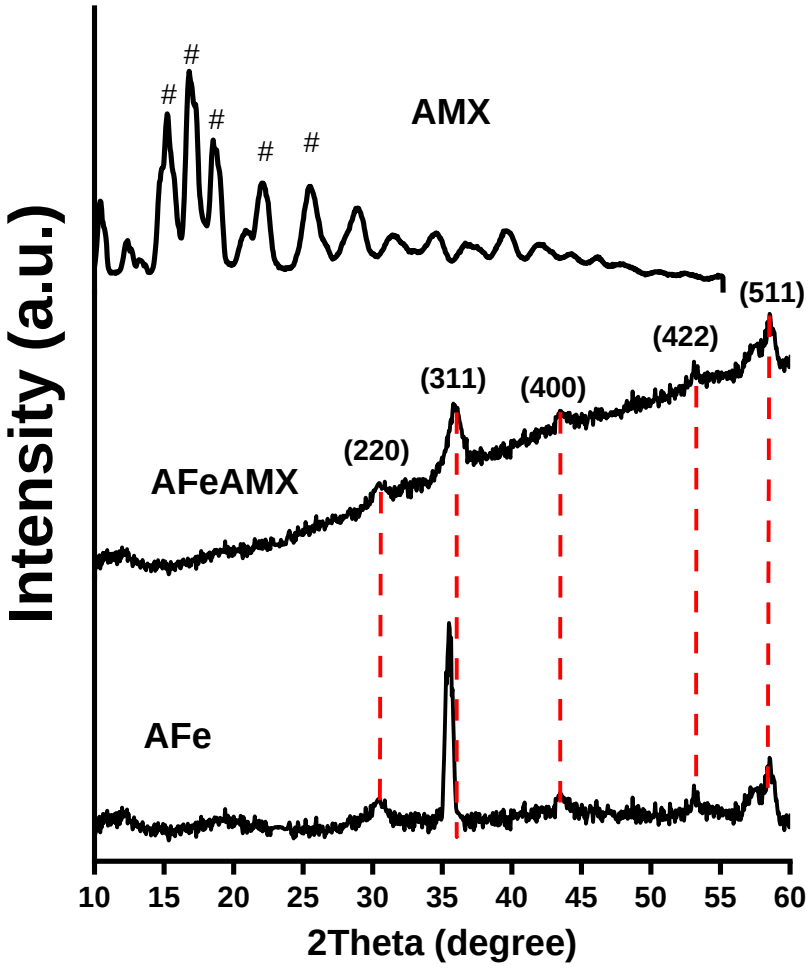

Figure 6: Powdered X-ray diffractograms of AMX, AFe nanoparticles and AFeAMX composite.

3.1.5 Surface functional analysis

The surficial characteristics of bare magnetite NPs, AFe and AFeAMX composite were elucidated using FTIR technique, Figure 7. In the FTIR spectrum of bare magnetite NPs, the Fe-O functional group, which is a characteristic vibrational mode of Fe_3O_4, was observed around 509 cm^{-1}, and there were no vibrational modes due to Fe_2O_3 at 632cm^{-1}, Figure 7a, indicating that the prepared

sample is pure Fe_3O_4. In the FTIR spectrum of AFe, the presence of OH stretching (3028-3602 cm^{-1}), CO stretching (1343 cm^{-1}), and OH bending (1563 cm^{-1}) due to sodium alginate, as well as the vibrational mode of Fe-O at 524 cm^{-1} of magnetite NPs, indicates that alginate was successfully bounded to magnetite NPs, Figure 7b. The presence of AMX significantly increased the vibrational peaks of oxygen functionalities in the AFeAMX spectrum, Figure 7c. This provides additional evidence for the successful loading of AMX onto alginate-magnetite composite.

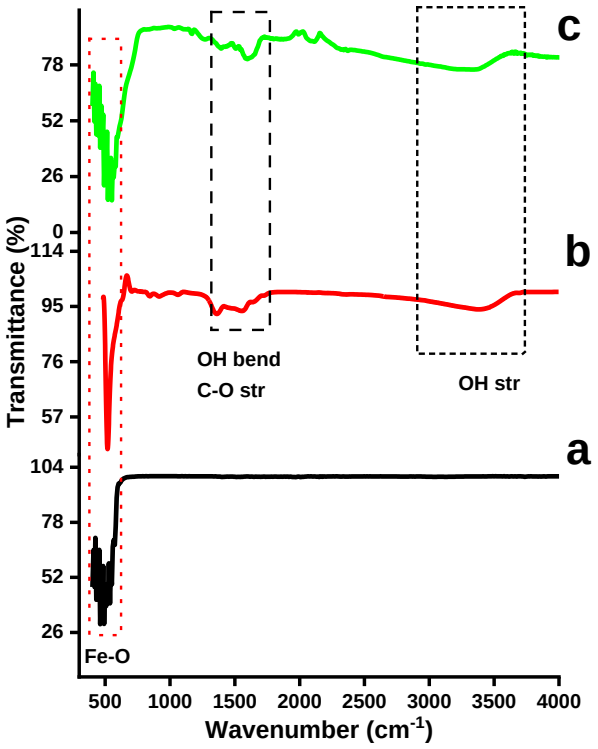

Figure 7: FT-IR spectra of (a) bare magnetite NPs, (b) alginate-capped magnetite NPs, and (c) AMX loaded alginate-magnetite composite.

3.1.6 Thermal analysis of bare magnetite and AFe nanoparticles

The amount of alginate loaded (wt%) on magnetite NP in the AFe composite was determined using thermogravimetry analysis (TGA) under N_2 atmosphere from 30 - 800 °C at 25.00 °C/min, Figure 8. The TGA plot of bare magnetite NP shows a small weight loss of 6.5% at onset temperature above 180 ^oC due to the loss of trapped water molecules, followed by weight loss from 255 to 800 ^oC with a total mass loss of 53.1%. The TGA curve of Alginate capped magnetite NPs (AFe) shows

three degradation processes at 160 °C, 278 °C, and 514 °C, respectively, corresponding to the loss of physisorbed water molecules, decarbonylation of sodium alginate matrix, and final decomposition of organic-carbon residues, releasing H_2O, CO_2, and other smaller molecules from AFe [31]. At 800°C, AFe NP degraded completely with a total mass of 63.6%, implying that the amount of sodium alginate on bare magnetite NP was 10.5%.

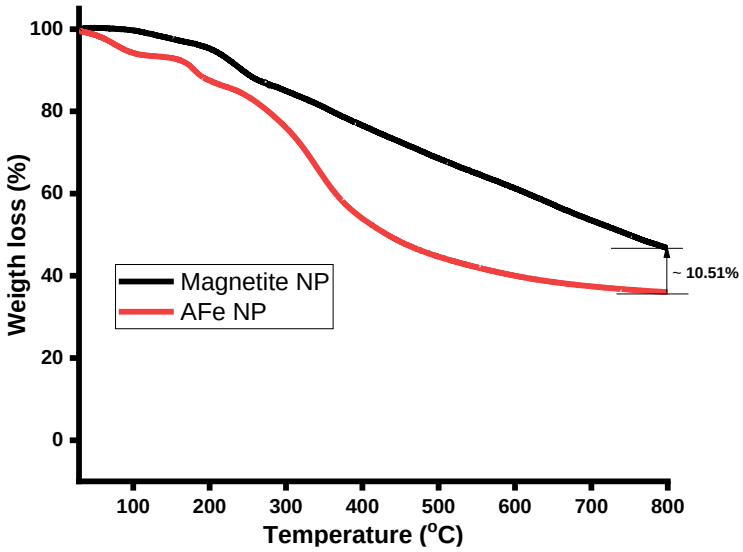

Figure 8: Thermogravimetry curves of bare magnetite NP, and alginate loaded magnetite (Afe) NP.

3.1.7 Surface area and structural analysis

The surface textural characteristics of as-synthesized AFe nanoparticles before and after composition with AMX are also elucidated using Brunauer–Emmett–Teller (BET) technique. The loops between 0.45-1.0 P/Po in the N_2 adsorption-desorption isotherms of AFe and AFeAMX suggest that the samples displayed type IV isotherms with H3 hysteresis loops, which is an indicative of mesoporous nanomaterials, Figure 9. The nitrogen uptake by AFe was moderate at lower relative pressure between 0.0 and ~0.51 P/Po, followed by rapid N_2 uptake to reach a maximum relative pressure of 1.0 P/Po, corresponding to adsorbed volume of 18.94 cm^3/g. In contrast, N_2 adsorption of AFeAMX composite increased slowly from 0.0 to 0.8 P/Po and rapidly increased to its optimum adsorption value of 5.95 cm^3/g. The results suggests that the presence of sodium alginate endowed AFe nanoparticles with higher mesoporosity and hence have higher textural surface area of 3.92 m^2/g than AFeAMX with surface area of 2.36 m^2/g. The AMX-

alginate magnetite matrix interactions limit active pore sites, resulting in a reduced surface area of the AFeAMX composite.

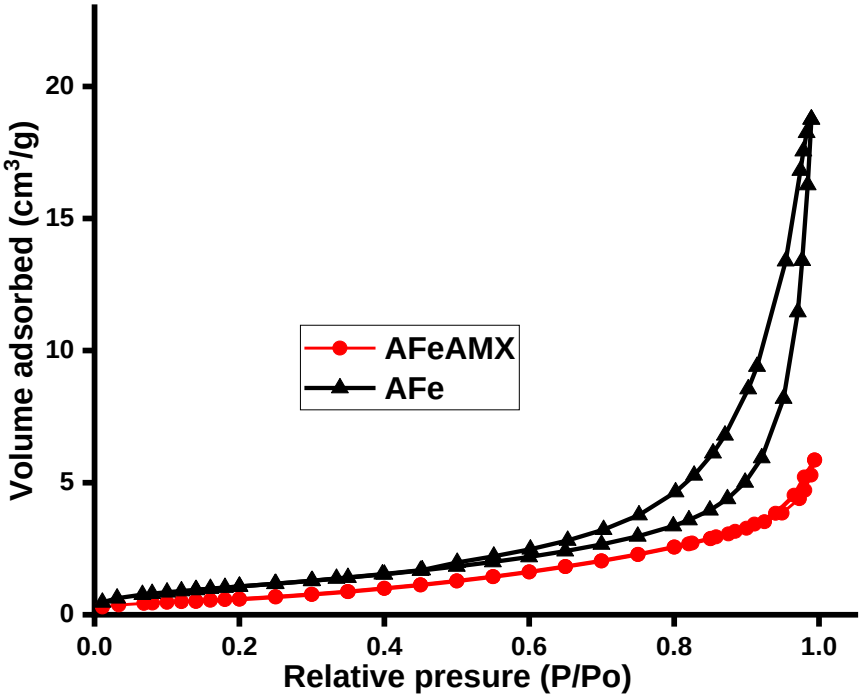

Figure 9: Brunauer–Emmett–Teller (BET) for measuring surface textures of AFe nanoparticles and AFeAMX composite.

3.1.8 Elemental composition of alginate-capped magnetite (AFe) nanoparticles

The elemental component of the prepared AFe nanoparticles was determined using the X-ray photoelectron spectroscopy (XPS) technique. The high-resolution for XPS survey of Fe element shows the presence of Fe 2p3/2 and Fe 2p1/2 peaks at two distinct binding energies of 711.4 eV and 724.8 eV, respectively, Figure 10. The spin orbit separation of the two binding energies is 13.53 ($\Delta_{BE}=$ 13.6 eV), and it is comsistent with the literature standard value for the Fe^{3+} ionization state during the preparation of Fe_3O_4 nanoparticles [32–34]. The absence of a satellite band at 719 eV in the XPS pattern of AFe, which indicates the formation of γ-Fe_2O_3, strongly suggests that the AFe nanoparticles are entirely made of Fe_3O_4 and not γ-Fe_2O_3 [35, 36]. The prominent signal peak at 284.9 eV in the XPS high resolution C1s spectrum is attributed to a mixture of C–C and carbonyl groups of sodium alginate, which was used as both a stabilizing and capping agent [37]. The O 1s high-resolution pattern has a sharp peak at 532.1 eV and a lesser peak at 529.4 eV, which are

attributed to the presence of O_2^- in magnetite and $O-H$ due to adsorbed water or alginate molecules [38, 39], respectively. Survey scan analysis of Na element in the AFe nanoparticles indicate the presence of Na 1s peak with binding energy of 1072.2 eV due to Na-O bond in sodium alginate [40].

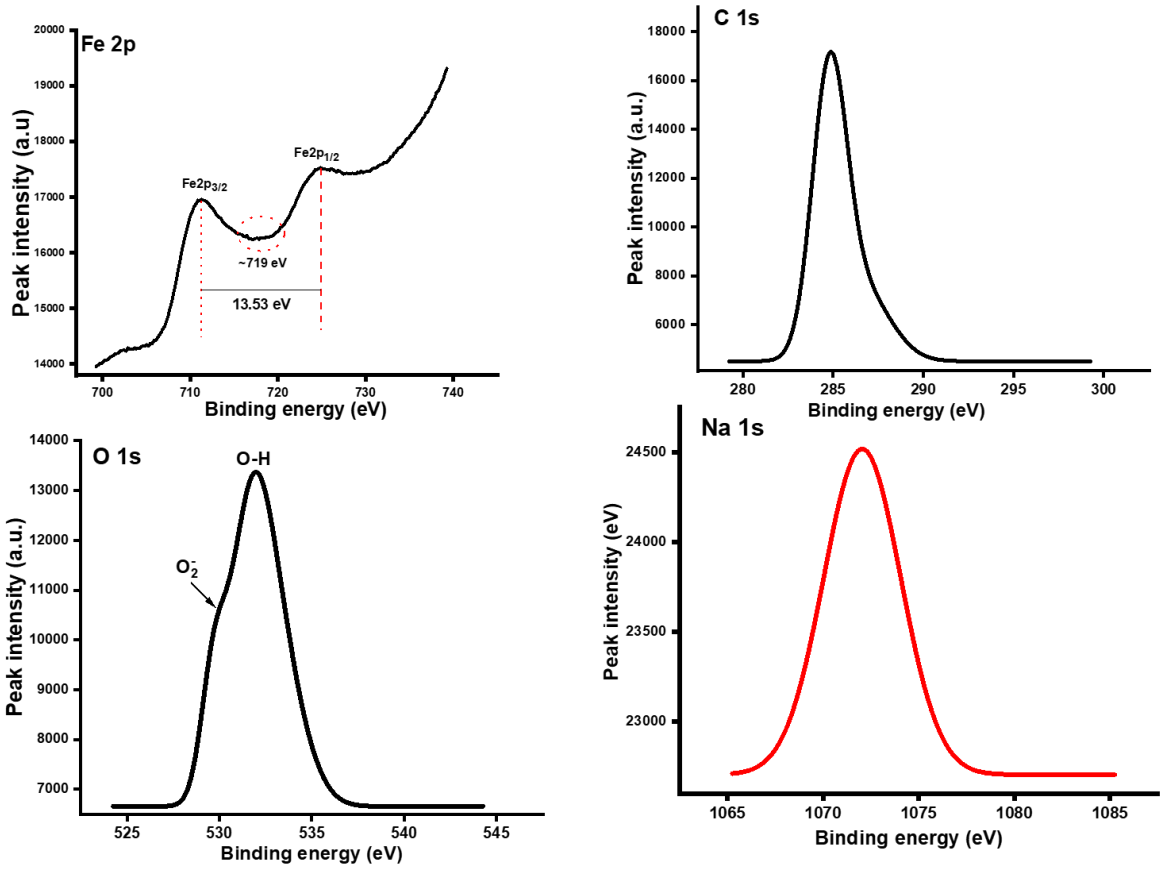

Figure 10: X-ray photoelectron spectroscopy (XPS) high-resolution spectra of Fe 2p (2p1/2 and Fe 2p3/2), C 1s, O 1s and Na 1s.

3.1.9 Determination of pH of point of Zero charge (pHpzc).

The adsorption efficiency of adsorbent for adsorbate removal in solution are often dictated by their net surface charges at different solution pH [41]. Thus, the net surface charge of the adsorbent, AFe, at different pH was determined using a pH of point zero charge (pHpzc) method [41, 42]. Figure 11 shows the plot of $\Delta pH\,(pH_o - pH_f)$ againstpH_o, and from which the point of intersection, that is, $\Delta pH = 0$ at pH 8.35 gave the PZC of AFe. The observed result suggests that AFe nanocomposite has net cationic surface charge at pH below 8.35 and overall anionic surface

charge at pH > 8.35. Amoxicillin structure has three distinct functional groups (NH_2, COOH and OH) which can undergo ionization to enable amoxicillin exist in different forms and at different pH in aqueous solution [43–46]. Literature surveys show that in aqueous solution, amoxicillin species occur as AMX^+, $AMX^{\pm}$ and AMX^- at pH $1-2, 3-8$ and $9-12$, respectively [43–46]. In order to ensure strong electrostatic interaction between AFe and AMX, loading of AMX onto AFe was conducted at pH 6 and 7.4, which corresponds to the pH at which AMX is in its zwitterion form (pH $= 3.0-8.0$) [46, 47], and the AFe has net cationic surface charge.

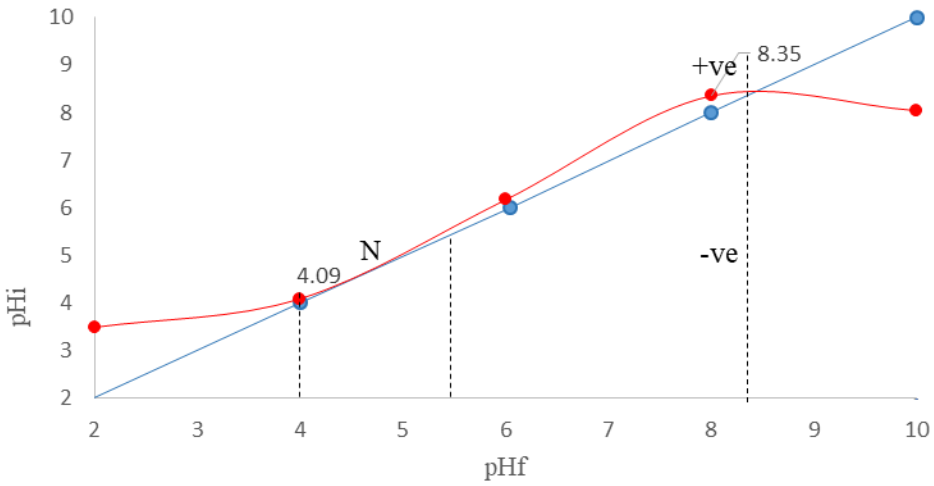

Figure 11: Plot showing the plot of pH of point zero charge for AFe nanocomposite.

3.2.0 AMX loading capacity and entrapment efficiency

The encapsulation efficiency (EE) refers to the percent weight ratio of the active components of amoxicillin adsorbed by the nanocomposite to the total weight of the AMX fed for adsorption studies. From **Eqn. 1**, the encapsulation efficiency of AMX via adsorption was calculated to be ca. 97.3%, and within the same value reported for in vitro evaluation of amoxicillin-alginate-coated chitosan microparticles by Onuigbo *et al.* [15]. Enhanced uptake of AMX by AFe composite in solution could be attributed to a number of factors such as van der Waals interactions, hydrogen bonding, pi-pi interactions and electrostatic attraction between negatively charged sodium alginate and positively charged NH_2 group on amoxicillin structure [48]. The relatively large surface area of AFe nanocomposite also plays prominent role in the sorption of AMX in aqueous solution. The reduced surface area of AFe composite after the loading is an indication that the pores on AFe composite were filled with AMX after adsorption. The loading capacity which

is the percent ratio of adsorbed AMX per unit mass of AFe nanoparticles was calculated as 43.2% using **Eqn. 2**.

3.2.1 In vitro release of AMX from AFeAMX

Figure 11 shows the cumulative *in vitro* release profile of AMX from phosphate buffer saline solutions of AMX-loaded AFe at pH 6.2 and 7.4 for 96 h. Under the same experimental conditions, the release rate of AMX at pH 6.2 is relatively higher than the release rate of AMX at alkaline pH of 7.4, suggesting that the release of AMX is pH-dependent and that their release is strongly affected by solution pH. The percentage release of the AMX from the formulation at pH 6.2 and 7.4 after 96 h are 86.4 and 74.6%, respectively. As demonstrated in Figure 12, the cumulative release of AMX followed two steps at pH 6.2 and 7.4: (i) initial burst release of AMX which lasted for 2 h due to the loosely held AMX molecules to the surface of AFe nanoparticles; and (ii) continuous release of AMX lasting up to 96 h, which was due to slower diffusion of the residual AMX that are encapsulated within the pores of the adsorbent [49, 50].

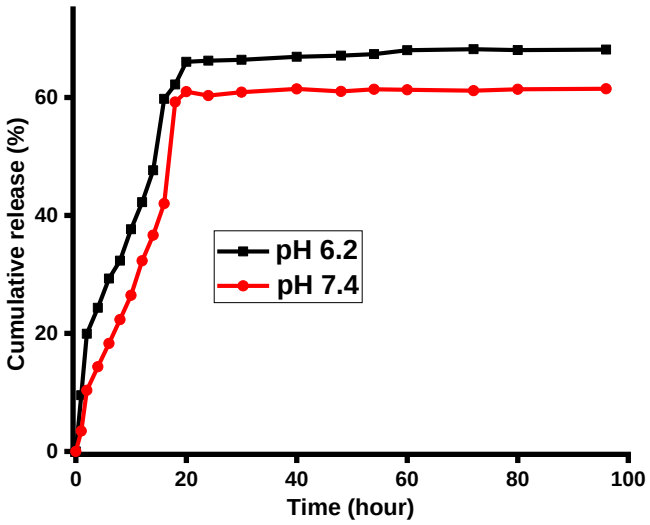

Figure 12: Cumulative *in vitro* release profile of AMX from phosphate buffer saline solutions of AMX-loaded AFe at pH 6.2 and 7.4.

3.2.2 Antimicrobial activity of AFeAMX

The efficacy of the prepared AFe sample before and after it was composited with amoxicillin as nano AFe-AMX formulation were tested against *Listeria monocytogenes* and *Salmonella typhi*,

which are gram-positive and gram-negative bacteria, respectively. *Salmonella typhi* infections, such as typhoid fever, have been linked to consuming sewage-contaminated food or water, and untreated or poorly treated *S. typhi* infections can cause liver damage, and internal bleeding [51]. *L. monocytogenes* infections, like *S. typhi*, are spread by consuming infected food products such as fish, meat, and vegetables, and can result in listeriosis [52]. The antibacterial activities of the prepared samples against the tested organisms after 48 h are measured in terms of zones of inhibition (measured in mm) around the agar plate, Figure 13. The MIC and MBC values are summarized in Table 1. At lower MIC and MBC values of 5 µg/mL and 10 µg/mL, respectively, the inhibitory zones of conventional antibiotics (AMX) against *L. monocytogenes*, a gram-positive bacteria, are much higher than *S. typhi*, which had higher MIC and MBC values. This indicates that *S. typhi* has a greater antimicrobial resistance level to amoxicillin. This finding is in line with prior research on antimicrobial resistance gram-negative bacteria to amoxicillin [53]. The minimum inhibitory concentration (MIC) values for sodium alginate alone were approximately 150 µg/mL, with no detectable inhibitory zones against the microorganisms tested, implying that sodium alginate alone is incapable of suppressing bacterial growth. According to literature report, sodium alginate has little or no antibacterial activity against both gram-positive and gram-negative bacteria [54]. Thus, sodium alginate serves to provide active sites for AMX adsorption and maintain its slow and controlled release during interaction of AFeAMX with microorganisms. There were no obvious differences in the observed zone of inhibition of bare magnetite NPs and alginate-capped magnetite NPs, as the latter had no effect on the studied microorganism, so the MIC and MBC values of the former were reported in Table 1. The bare magnetite NPs showed slightly higher growth inhibitory effect on gram-negative bacterium (*S. typhi*) compared to *L. monocytogenes*. Higher toxicity effects of iron based nanomaterial against gram-negative bacteria than gram-positive bacteria have been reported [55]. Interestingly, the combination of sodium alginate-capped magnetite (AFe) and AMX showed significantly antimicrobial inhibitory growth against *L. monocytogenes*and *S. typhi* at MIC values of 10 and 30 µg/mL, respectively. The zone of inhibition of AFeAMX was slightly higher against *L. monocytogenes* at $27 - 32$ mm compared to *S. typhi* with $\approx 17 \pm 1.1$ mm zone of inhibition after 48 h. This suggests that the response of bacteria against antibiotics is determined by the specific interactions between the bacterial metabolic features and nature of the antibiotics.

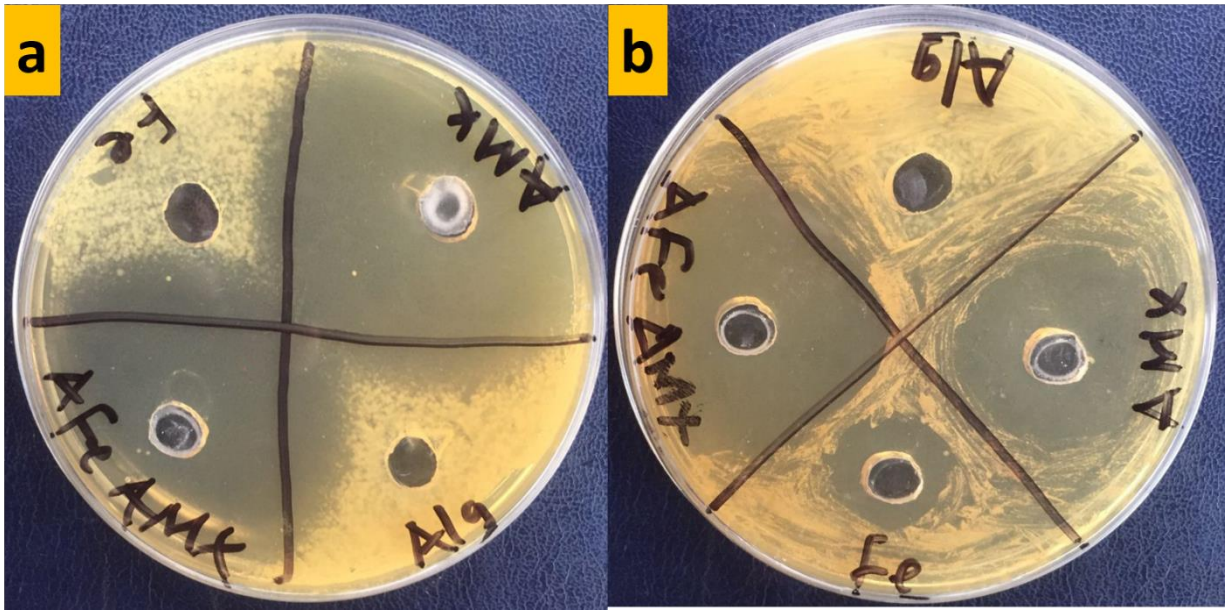

Figure 13: Images showing zone of inhibition of alginate, bare magnetite NPs, AMX and AFeAMX composite against (a) *L. monocytogenes* and (b) *S. typhi.*

Table 1: Antimicrobial activity of bare magnetite nanoparticles, sodium alginate, amoxicillin, and amoxicillin-capped magnetite nanocomposite against *L. monocytogenes* and *S. typhi*, as determined using the agar diffusion method

	Listeria monocytogenes				***Salmonella typhi***			
Sample	MIC (µg/mL)	MBC (µg/mL)	Inhibitory zone (mm)		MIC (µg/mL)	MBC (µg/mL)	Inhibitory zone(mm)	
			24 h	48 h			24 h	48 h
AFe[a]	60	100	6 ± 0.2	7 ± 0.3	70	140	9 ± 0.3	9 ± 0.2
Alg[b]	150	200	2 ± 0.1	2 ± 0.1	150	200	1 ± 0.1	2 ± 0.1
AMX[c]	5	10	29 ± 0.5	26 ± 0.5	20	40	19 ± 0.4	18 ± 0.4
AFeAMX	10	20	27± 0.6	32 ± 0.6	30	50	17 ± 0.4	19 ± 0.3

[a]bare magnetite nanoparticles, [b]sodium alignate, [c]amoxillin as standard antibiotic.

3.2.3 Mechanism of antimicrobial action of AFeAMX

Amoxicillin is a common antibiotic whose mode of action on microorganisms is to disrupt the cross-linking of the peptidoglycan (PG) layer, which is a macromolecular polymer and a key component in the formation of bacterial cell walls [56, 57]. Figures 14 a & b show representative schematic diagrams for cell wall formation in the absence of AMX and bacterial cell wall disruption in the presence of AMX. The alternating peptide chains of amino acids, N-acetylglucosamine (GlcNA) and N-acetylmuramic acid (MurNAc), cross-linked to form a stable and rigid mesh-like structure of peptidoglycan (PG) layer to protect bacterial cell walls from external pressors in the absence of AMX, Figure 14a. However, during constant and controlled release of AMX from AFeAMX, the AMX binds to the active sites of the penicillin binding proteins (transpeptidases) of the microorganisms, interrupting the transpeptidases steps and disrupting the cross-linking of GlcNA and N-MurNAc, Figure 14b. Because PG layers are critical components for microorganism protection, disruption of transpeptidase steps indicates that bacterial cell walls will be unable to protect the organism from external stressors or osmotic pressure changes, resulting in bacterial lysis or death [56, 57].

In addition to disrupting bacterial cell walls through controlled release of AMX, magnetite NPs, which serves as solid support for AMX in this work, is also a potent antimicrobial therapy against tested microbes. Magnetite nanomaterials, like other metal-based nanomaterials [58, 59], can inhibit microorganisms or induce bactericidal effects via three distinct mechanisms: (i) intracellular metal ions penetration into cell walls arising from adhesion of metal NPs to the cell membrane, (ii) oxidative stress induced-cellular damage to mitochondria, proteins and DNA by the accumulation of reactive oxygen species (ROS), and (iii) the leakage of cellular components of microbes, Figure 15. The current findings are consistent with those of prior studies, which revealed that combination of antibiotics with alginate or magnetite nanoparticles had synergistic effects against microorganisms [11, 12, 60–63].

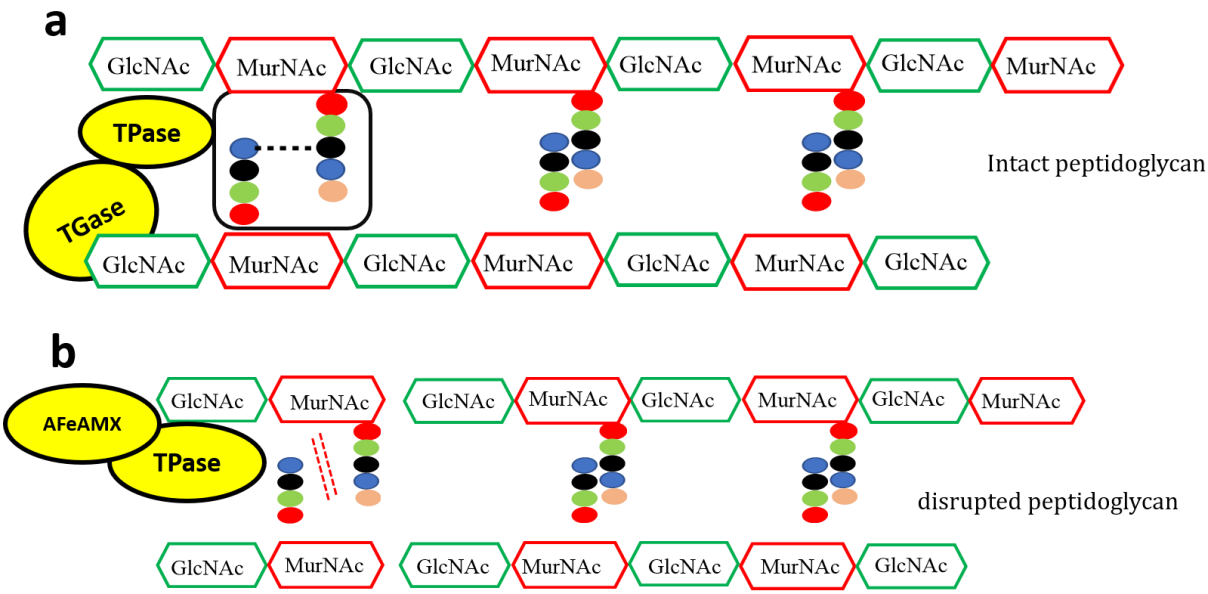

Figure 14: Schematic diagrams for (a) cell wall formation in the absence of AFeAMX and (b) bacterial cell wall disruption in the presence of AFeAMX.

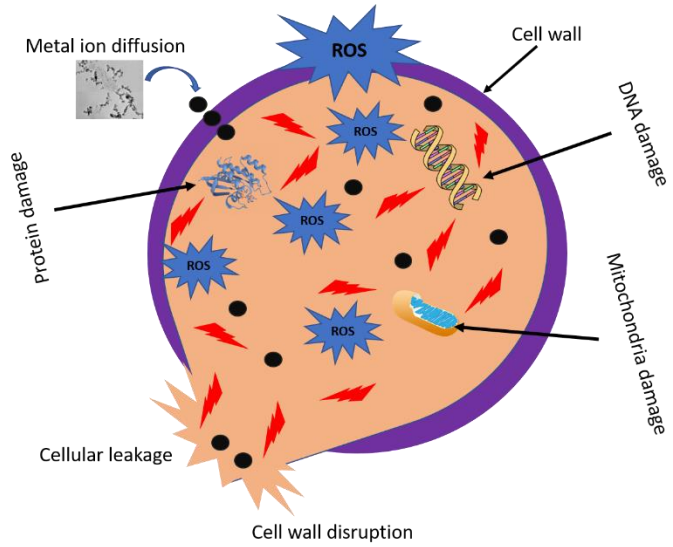

Figure 15: Illustration of mechanisms of antimicrobial activity of AFeAMX against pathogens.

Conclusion

The present work describes the synthesis of magnetite nanoparticles stabilized with sodium alginate. Amoxicillin, an antibiotic, was encapsulated on the as-prepared alginate-magnetite composite to afford amoxicillin-loaded magnetite formulation (abbreviated as AFeAMX). The in vitro release profiles indicate that 86.4 % and 74.6% of AMX are respectively released from the

formulation at pH 6.2 and 7.4 after 96 h. Antimicrobial activities of magnetite nanoparticles before and after loading of AMX were carried out against *Listeria monocytogenes* and *Salmonella typhi*, which are gram-positive and gram-negative bacteria, respectively. The antimicrobial efficacy of AFeAMX is more pronounced with significantly higher inhibitory effects against *L. monocytogenes* at lower MIC and MBC values than against *S. typhi*, which was tested at higher values of MIC and MBC. We hypothesized that AMX binds to the bacterial enzyme and disrupts the cross-linking of the peptidoglycan layer, which is a critical component responsible for cell wall synthesis, resulting in bacterial death. Furthermore, the presence of magnetite as a substrate for AMX and alginate had significant bactericidal effects on microorganisms via metal ion diffusion into cell walls, oxidative stress-induced-cellular damage to the cell membrane, and leakage of microbe cellular components.

Conflict of interest

The authors declare that there is no conflict of interests regarding the publication of this paper.

Funding statement

No funding information provided in the manuscript.

Ethics statement/approval

The research does not involve humans and animals

Informed consent

Not applicable

REFERENCES

1. Bayda, S., Adeel, M., Tuccinardi, T., Cordani, M., & Rizzolio, F. (2020). The history of nanoscience and nanotechnology: From chemical-physical applications to nanomedicine. *Molecules*, *25*(1), 1–15. https://doi.org/10.3390/molecules25010112

2. Patra, J. K., Das, G., Fraceto, L. F., Campos, E. V. R., Rodriguez-Torres, M. D. P., Acosta-Torres, L. S., … Shin, H. S. (2018). Nano based drug delivery systems: Recent developments and future prospects 10 Technology 1007 Nanotechnology 03 Chemical Sciences 0306 Physical Chemistry (incl. Structural) 03 Chemical Sciences 0303 Macromolecular and Materials Chemistry 11 Medical and He. *Journal of Nanobiotechnology*, *16*(1), 1–33. https://doi.org/10.1186/s12951-018-0392-8

3. Jong, W. H. De, & Paul, J. B. (2008). Drug delivery and nanoparticles : Applications and hazards. *International Journal of Nanomedicine*, *3*(2), 133–149.

4. Weng, J., Tong, H. H. Y., & Chow, S. F. (2020). In vitro release study of the polymeric drug nanoparticles: Development and validation of a novel method. *Pharmaceutics*, *12*(8), 1–18. https://doi.org/10.3390/pharmaceutics12080732

5. Natarajan, J. V., Nugraha, C., Ng, X. W., & Venkatraman, S. (2014). Sustained-release from nanocarriers: A review. *Journal of Controlled Release*, *193*, 122–138. https://doi.org/10.1016/j.jconrel.2014.05.029

6. B. Alberts, A. Johnson, J. Lewis, M. Raff, K. Roberts, P. W. (2002). *Molecular Biology of the Cell*. New York: Garland Science.

7. Zorofchian Moghadamtousi, S., Abdul Kadir, H., Hassandarvish, P., Tajik, H., Abubakar, S., & Zandi, K. (2014). A review on antibacterial, antiviral, and antifungal activity of curcumin. *BioMed Research International*, *2014*. https://doi.org/10.1155/2014/186864

8. Xu, C., Akakuru, O. U., Zheng, J., & Wu, A. (2019). Applications of iron oxide-based magnetic nanoparticles in the diagnosis and treatment of bacterial infections. *Frontiers in Bioengineering and Biotechnology*, *7*(JUN), 1–15. https://doi.org/10.3389/fbioe.2019.00141

9. M. B. El Din Mohamed, F. I. A. El-Ela, R. K. Mahmoud, A. A. Farghali, S. Gamil, S. A. A. A. A. (2022). Cefotax-magnetic nanoparticles as an alternative approach to control Methicillin-Resistant Staphylococcus aureus (MRSA) from different sources. *Sci. Rep.*, *12*, 624.

10. S. Bucak, B. Yavuztürk, and A. D. S. (2012). *"Magnetic Nanoparticles: Synthesis, Surface Modifications and Application in Drug Delivery", in Recent Advances in Novel Drug Carrier Systems.*

11. Hussein-Al-Ali, S. H., El Zowalaty, M. E., Hussein, M. Z., Geilich, B. M., & Webster, T. J. (2014). Synthesis, characterization, and antimicrobial activity of an ampicillin-conjugated magnetic nanoantibiotic for medical applications. *International Journal of Nanomedicine*, *9*(1), 3801–3814. https://doi.org/10.2147/IJN.S61143

12. Grumezescu, A. M., Gesta, M. C., Holban, A. M., Grumezescu, V., Vasile, B. S., Mogoanta, L., … Dan Mogosanu, G. (2014). Biocompatible Fe3O4 increases the efficacy of amoxicillin delivery against gram-positive and gram-negative bacteria. *Molecules*, *19*(4), 5013–5027. https://doi.org/10.3390/molecules19045013

13. Arakha, M., Pal, S., Samantarrai, D., Panigrahi, T. K., Mallick, B. C., Pramanik, K., … Jha, S. (2015). Antimicrobial activity of iron oxide nanoparticle upon modulation of nanoparticle-bacteria interface. *Scientific Reports*, *5*, 1–12. https://doi.org/10.1038/srep14813

14. Zhu, N., Ji, H., Yu, P., Niu, J., Farooq, M. U., Akram, M. W., … Niu, X. (2018). Surface modification of magnetic iron oxide nanoparticles. *Nanomaterials*, *8*(10), 1–27. https://doi.org/10.3390/nano8100810

15. Onuigbo, E., Onugwu, A., Nwocha, M., Odiase, A., & Attama, A. (2016). Preparation and

in vitro evaluation of amoxicillin encapsulated in alginate-coated chitosan microparticles. *Tropical Journal of Pharmaceutical Research*, *15*(11), 2303–2309. https://doi.org/10.4314/tjpr.v15i11.2

16. Arora, S., Gupta, S., Narang, R. K., & Budhiraja, R. D. (2011). Amoxicillin loaded chitosan-alginate polyelectrolyte complex nanoparticles as mucopenetrating delivery system for H. pylori. *Scientia Pharmaceutica*, *79*(3), 673–694. https://doi.org/10.3797/scipharm.1011-05

17. Sutherland, R., Croydon, E. A. P., & Rolinson, G. N. (1972). Amoxycillin: A new Semi-synthetic Penicillin. *British Medical Journal*, *3*(5817), 13–16. https://doi.org/10.1136/bmj.3.5817.13

18. Niculescu, A. G., Chircov, C., & Grumezescu, A. M. (2022). Magnetite nanoparticles: Synthesis methods – A comparative review. *Methods*, *199*(April 2021), 16–27. https://doi.org/10.1016/j.ymeth.2021.04.018

19. A. Ali1, T. Shah, R. Ullah, P. Zhou, M. Guo, M. Ovais, Z. Tan, Y. R. (n.d.). Review on Recent Progress in Magnetic Nanoparticles: Synthesis, Characterization, and Diverse Applications. *Methods*, *9*, 629054.

20. Hammadi, N. I., Abba, Y., Hezmee, M. N. M., Razak, I. S. A., Jaji, A. Z., Isa, T., … Zakaria, M. Z. A. B. (2017). Formulation of a Sustained Release Docetaxel Loaded Cockle Shell-Derived Calcium Carbonate Nanoparticles against Breast Cancer. *Pharmaceutical Research*, *34*(6), 1193–1203. https://doi.org/10.1007/s11095-017-2135-1

21. Mailafiya, M. M., Abubakar, K., Danmaigoro, A., Chiroma, S. M., Rahim, E. B. A., Moklas, M. A. M., & Zakaria, Z. A. B. (2019). Evaluation of in vitro release kinetics and mechanisms of curcumin-loaded cockle shell-derived calcium carbonate nanoparticles. *Biomedical Research and Therapy*, *6*(12), 3518–3540. https://doi.org/10.15419/bmrat.v6i12.580

22. Ataklti, A., Alemu, K., & Abebe, B. (2016). Study of the self-association of amoxicillin, thiamine and the hetero-association with biologically active compound chlorgenic acid. *African Journal of Pharmacy and Pharmacology*, *10*(18), 393–402. https://doi.org/10.5897/ajpp2016.4542

23. Rouhani, P., Govindaraju, N., Iyer, J. K., Kaul, R., Kaul, A., & Singh, R. N. (2020). Functionalized diamond nanoparticles as a drug delivery system: Loading and release study. *Medical Devices & Sensors*, *3*(1), 1–14. https://doi.org/10.1002/mds3.10057

24. A. Danmaigoro, G.T. Selvarajah, M.H. Noor, R. Mahmud, M. Z. Z. (n.d.). Development of cockleshell (Anadara Granosa) derived CaCO3 nanoparticle for doxorubicin delivery. *J. Comput. Theor. Nanosci*, *14*(10), 5074–5086.

25. Akinpelu, D. A., & Onakoya, T. M. (2006). Antimicrobial activities of medicinal plants used in folklore remedies in south-western. *African Journal of Biotechnology*, *5*(11), 1078–1081.

26. Saptarini, N. M., Warya, S., Sari, A. D. P., & Setyarini, A. (2015). Stability studies of Amoxicillin and Gentamicin injection in intravenous infusions. *Journal of Young Pharmacists*, *7*(3), 250–256. https://doi.org/10.5530/jyp.2015.3.16

27. Awasthi, R., Kulkarni, G. T., Pawar, V. K., & Garg, G. (2012). Optimization studies on gastroretentive floating system using response surface methodology. *AAPS PharmSciTech*, *13*(1), 85–93. https://doi.org/10.1208/s12249-011-9730-y

28. Arivarasan, V. K., Loganathan, K., Venkatesan, J., & Chaskar, A. C. (2021). 'Synergistic-Cidal' Effect of Amoxicillin Conjugated Silver Nanoparticles Against Escherichia coli. *BioNanoScience*, *11*(2), 506–517. https://doi.org/10.1007/s12668-021-00832-7

29. Brittain, H. G. (2005). Solid-state fluorescence of the trihydrate phases of ampicillin and amoxicillin. *AAPS PharmSciTech*, *6*(3), 444–448. https://doi.org/10.1208/pt060355

30. Bankole, O. M., & Nyokong, T. (2016). Comparative studies on photophysical and optical limiting characterizations of low symmetry phthalocyanine linked to Fe3O4-Ag core-shell or hybrid nanoparticles. *New Journal of Chemistry*, *40*(12), 10016–10027. https://doi.org/10.1039/c6nj01511e

31. Liu, Y., Zhao, J. C., Zhang, C. J., Guo, Y., Cui, L., Zhu, P., & Wang, D. Y. (2015). Bio-based nickel alginate and copper alginate films with excellent flame retardancy: Preparation, flammability and thermal degradation behavior. *RSC Advances*, *5*(79), 64125–64137. https://doi.org/10.1039/c5ra11048c

32. Qu, B., Sun, Y., Liu, L., Li, C., Yu, C., Zhang, X., & Chen, Y. (2017). Ultrasmall Fe2O3 nanoparticles/MoS2 nanosheets composite as high-performance anode material for lithium ion batteries. *Scientific Reports*, *7*(February), 1–11. https://doi.org/10.1038/srep42772

33. Biesinger, M. C., Lau, L. W. M., Gerson, A. R., & Smart, R. S. C. (2010). Resolving surface chemical states in XPS analysis of first row transition metals, oxides and hydroxides: Sc, Ti, V, Cu and Zn. *Applied Surface Science*, *257*(3), 887–898. https://doi.org/10.1016/j.apsusc.2010.07.086

34. Jiang, Y., Zhang, D., Li, Y., Yuan, T., Bahlawane, N., Liang, C., … Yan, M. (2014). Amorphous Fe2O3 as a high-capacity, high-rate and long-life anode material for lithium ion batteries. *Nano Energy*, *4*, 23–30. https://doi.org/10.1016/j.nanoen.2013.12.001

35. Teng, X., Black, D., Watkins, N. J., Gao, Y., & Yang, H. (2003). 1542.NanoLett.2003,3,261.pdf.

36. Tian, Y., Yu, B., Li, X., & Li, K. (2011). Facile solvothermal synthesis of monodisperse Fe3O4 nanocrystals with precise size control of one nanometre as potential MRI contrast agents. *Journal of Materials Chemistry*, *21*(8), 2476–2481. https://doi.org/10.1039/c0jm02913k

37. Tong, Z., Chen, Y., Liu, Y., Tong, L., Chu, J., Xiao, K., … Chu, X. (2017). Preparation, characterization and properties of alginate/poly(γ-glutamic acid) composite microparticles. *Marine Drugs*, *15*(4). https://doi.org/10.3390/md15040091

38. Gao, W., Li, S., Huo, H., Li, F., Yang, Y., Li, X., … Li, R. (2017). Investigation of the crystal structure of Cu-Fe bimetal oxide and their catalytic activity for the Baeyer–Villiger oxidation reaction. *Molecular Catalysis*, *439*, 108–117. https://doi.org/10.1016/j.mcat.2017.06.027

39. Manatunga, D. C., de Silva, R. M., de Silva, K. M. N., Wijeratne, D. T., Malavige, G. N., & Williams, G. (2018). Fabrication of 6-gingerol, doxorubicin and alginate hydroxyapatite into a bio-compatible formulation: Enhanced anti-proliferative effect on breast and liver cancer cells. *Chemistry Central Journal*, *12*(1), 1–13. https://doi.org/10.1186/s13065-018-0482-6

40. Journal, S., & Earth, O. F. (2017). X-ray Photoelectron Spectroscopy study of so-called "Larimar", blue pectolite from the Dominican Republic. *SDRP Journal of Earth Sciences & Environmental Studies*, *1*(2), 0–4. https://doi.org/10.25177/jeses.1.2.4

41. Samarghandi, M. R., Al-Musawi, T. J., Mohseni-Bandpi, A., & Zarrabi, M. (2015). Adsorption of cephalexin from aqueous solution using natural zeolite and zeolite coated with manganese oxide nanoparticles. *Journal of Molecular Liquids*, *211*, 431–441. https://doi.org/10.1016/j.molliq.2015.06.067

42. PanelMarekKosmulski, A. links open overlay. (2021). The pH dependent surface charging and points of zero charge. IX. Update. *Advances in Colloid and Interface Science*, *296*, 102519.

43. Moussavi, G., Alahabadi, A., Yaghmaeian, K., & Eskandari, M. (2013). Preparation, characterization and adsorption potential of the NH4Cl-induced activated carbon for the removal of amoxicillin antibiotic from water. *Chemical Engineering Journal*, *217*, 119–128. https://doi.org/10.1016/j.cej.2012.11.069

44. Putra, E. K., Pranowo, R., Sunarso, J., Indraswati, N., & Ismadji, S. (2009). Performance of activated carbon and bentonite for adsorption of amoxicillin from wastewater: Mechanisms, isotherms and kinetics. *Water Research*, *43*(9), 2419–2430. https://doi.org/10.1016/j.watres.2009.02.039

45. Martins, A. C., Pezoti, O., Cazetta, A. L., Bedin, K. C., Yamazaki, D. A. S., Bandoch, G. F. G., … Almeida, V. C. (2015). Removal of tetracycline by NaOH-activated carbon produced from macadamia nut shells: Kinetic and equilibrium studies. *Chemical Engineering Journal*, *260*, 291–299. https://doi.org/10.1016/j.cej.2014.09.017

46. Pezoti, O., Cazetta, A. L., Bedin, K. C., Souza, L. S., Martins, A. C., Silva, T. L., … Almeida, V. C. (2016). NaOH-activated carbon of high surface area produced from guava seeds as a high-efficiency adsorbent for amoxicillin removal: Kinetic, isotherm and thermodynamic studies. *Chemical Engineering Journal*, *288*, 778–788. https://doi.org/10.1016/j.cej.2015.12.042

47. Adriano, W. S., Veredas, V., Santana, C. C., & Gonçalves, L. R. B. (2005). Adsorption of amoxicillin on chitosan beads: Kinetics, equilibrium and validation of finite bath models. *Biochemical Engineering Journal*, *27*(2), 132–137. https://doi.org/10.1016/j.bej.2005.08.010

48. Bao, H., Li, L., Gan, L. H., Ping, Y., Li, J., & Ravi, P. (2010). Thermo-and pH-responsive association behavior of dual hydrophilic graft chitosan terpolymer synthesized via ATRP and click chemistry. *Macromolecules*, *43*(13), 5679–5687. https://doi.org/10.1021/ma100894p

49. Sun, D., Xue, A., Zhang, B., Xue, X., Zhang, J., & Liu, W. (2016). Enhanced oral bioavailability of acetylpuerarin by poly(Lactide-co-glycolide) nanoparticles optimized using uniform design combined with response surface methodology. *Drug Design, Development and Therapy*, *10*, 2029–2039. https://doi.org/10.2147/DDDT.S108185

50. Dudhipala, N., & Veerabrahma, K. (2016). Candesartan cilexetil loaded solid lipid nanoparticles for oral delivery: Characterization, pharmacokinetic and pharmacodynamic evaluation. *Drug Delivery*, *23*(2), 395–404. https://doi.org/10.3109/10717544.2014.914986

51. Eng, S. K., Pusparajah, P., Ab Mutalib, N. S., Ser, H. L., Chan, K. G., & Lee, L. H. (2015). Salmonella: A review on pathogenesis, epidemiology and antibiotic resistance. *Frontiers in Life Science*, *8*(3), 284–293. https://doi.org/10.1080/21553769.2015.1051243

52. Matle, I., Mbatha, K. R., & Madoroba, E. (2020). A review of listeria monocytogenes from meat and meat products: Epidemiology, virulence factors, antimicrobial resistance and diagnosis. *Onderstepoort Journal of Veterinary Research*, *87*(1), 1–20. https://doi.org/10.4102/ojvr.v87i1.1869

53. Umair, M., & Siddiqui, S. A. (2020). Antibiotic Susceptibility Patterns of Salmonella Typhi and Salmonella Paratyphi in a Tertiary Care Hospital in Islamabad. *Cureus*, *12*(9). https://doi.org/10.7759/cureus.10228

54. Mohd Zin, F. A., Noor, A. M., Mohd Nasri, W. N. W., Roslan, N. N., Buniamin, N. A., Abdul Razab, M. K. A., … Rameshkumar, P. (2020). Synthesis of Sodium Alginate Graphene Oxide-Silver Film for Antibacterial Activity. *IOP Conference Series: Earth and Environmental Science*, *596*(1). https://doi.org/10.1088/1755-1315/596/1/012041

55. Gudkov, S. V., Burmistrov, D. E., Serov, D. A., Rebezov, M. B., Semenova, A. A., & Lisitsyn, A. B. (2021). Do iron oxide nanoparticles have significant antibacterial properties? *Antibiotics*, *10*(7), 1–23. https://doi.org/10.3390/antibiotics10070884

56. Upadhya R, K., Shenoy, L., & Venkateswaran, R. (2018). Effect of intravenous dexmedetomidine administered as bolus or as bolus-plus-infusion on subarachnoid anesthesia with hyperbaric bupivacaine. *Journal of Anaesthesiology Clinical Pharmacology*, *34*(3), 46–50. https://doi.org/10.4103/joacp.JOACP

57. Achparaki, M., Thessalonikeos, E., Tsoukali, H., Mastrogianni, O., Zaggelidou, E., Chatzinikolaou, F., … J. Poesen Additional. (2012). We are IntechOpen , the world ' s leading publisher of Open Access books Built by scientists , for scientists TOP 1 %. *Intech*, 13.

58. Hashem, A. H., Al Abboud, M. A., Alawlaqi, M. M., Abdelghany, T. M., & Hasanin, M. (2022). Synthesis of Nanocapsules Based on Biosynthesized Nickel Nanoparticles and

Potato Starch: Antimicrobial, Antioxidant, and Anticancer Activity. *Starch/Staerke*, *74*(1–2), 1–9. https://doi.org/10.1002/star.202100165

59. Amr M Shehabeldine, Amr H Hashem, Ahmed R Wassel, M. H. (2022). Antimicrobial and Antiviral Activities of Durable Cotton Fabrics Treated with Nanocomposite Based on Zinc Oxide Nanoparticles, Acyclovir, Nanochitosan, and Clove Oil. *Biotechnology and Applied Biochemistry*, *194*(2), 783–800.

60. Baltimore, R. S., Cross, A. S., & Dobek, A. S. (1987). The inhibitory effect of sodium alginate on antibiotic activity against mucoid and non-mucoid strains of pseudomonas aeruginosa. *Journal of Antimicrobial Chemotherapy*, *20*(6), 815–823. https://doi.org/10.1093/jac/20.6.815

61. Tayal, K., Kandav, G., Girotra, P., & Singh, S. K. (2015). Formulation and evaluation of chitosan coated magnetic nanoparticles of Amoxicillin trihydrate. *Der Pharmacia Lettre*, *7*(11), 241–251.

62. Wang, C., Xu, S., Zhang, K., Li, M., Li, Q., Xiao, R., & Wang, S. (2017). Streptomycin-modified Fe3O4–Au@Ag core–satellite magnetic nanoparticles as an effective antibacterial agent. *Journal of Materials Science*, *52*(3), 1357–1368. https://doi.org/10.1007/s10853-016-0430-6

63. Kumar, L., Brice, J., Toberer, L., Klein-Seetharaman, J., Knauss, D., & Sarkar, S. K. (2019). Antimicrobial biopolymer formation from sodium alginate and algae extract using aminoglycosides. *PLoS ONE*, *14*(3), 1–17. https://doi.org/10.1371/journal.pone.0214411